

1 Inhibiting *Mycobacterium tuberculosis* CoaBC by targeting a new allosteric
2 site.

3
4 Vitor Mendes^{1*}, Simon R. Green², Joanna C. Evans³, Jeannine Hess⁴, Michal Blaszczyk¹,
5 Christina Spry⁴, Owain Bryant¹, James Cory-Wright¹, Daniel S-H. Chan⁴, Pedro H.M.
6 Torres¹, Zhe Wang⁵, Sandra O'Neill², Sebastian Damerow², John Post², Tracy Bayliss²,
7 Sasha L. Lynch³, Anthony G. Coyne⁴, Peter C. Ray², Chris Abell⁴, Kyu Y. Rhee⁵, Helena
8 I. M. Boshoff⁶, Clifton E. Barry III^{3,6}, Valerie Mizrahi³, Paul G. Wyatt², Tom L.
9 Blundell^{1*}.

10
11 1 Department of Biochemistry, University of Cambridge, 80 Tennis Court Road, Cambridge, CB2 1GA,
12 UK

13 2 Drug Discovery Unit, College of Life Sciences, University of Dundee, Dow Street, Dundee, DD1 5EH,
14 Scotland, UK

15 3 MRC/NHLS/UCT Molecular Mycobacteriology Research Unit & DST/NRF Centre of Excellence for
16 Biomedical TB Research & Wellcome Centre for Infectious Diseases Research in Africa, Institute of
17 Infectious Disease and Molecular Medicine and Department of Pathology, Faculty of Health Sciences,
18 University of Cape Town, Anzio Road, Observatory 7925, South Africa

19 4 Department of Chemistry, University of Cambridge, Lensfield Road, Cambridge, CB2 1EW, UK

20 5 Division of Infectious Diseases, Weill Department of Medicine, Weill Cornell Medical College, New
21 York, NY 10065, USA

22 6 Tuberculosis Research Section, Laboratory of Clinical Immunology and Microbiology, National Institute
23 of Allergy and Infectious Disease, National Institutes of Health, 9000 Rockville Pike, Bethesda, Maryland
24 20892, USA

25

26 * To whom correspondence should be addressed

27 Vitor Mendes: vgm23@cam.ac.uk

28 Tom L. Blundell: tom@cryst.bioc.cam.ac.uk

29 **Abstract**

30 Coenzyme A (CoA) is a fundamental co-factor for all life, involved in numerous
31 metabolic pathways and cellular processes and its biosynthetic pathway has raised
32 substantial interest as a drug target against multiple pathogens including *Mycobacterium*
33 *tuberculosis*. The biosynthesis of CoA is performed in five steps. However, in the vast
34 majority of prokaryotes including *M. tuberculosis*, a single bifunctional protein, CoaBC,
35 catalyses the second and third steps. Depletion of CoaBC was found to be bactericidal in
36 *M. tuberculosis*. Here we report the first structure of a full length CoaBC, from the model
37 organism *Mycobacterium smegmatis*, describe how it is organised as a dodecamer and
38 regulated by CoA thioesters. A high-throughput biochemical screen focusing on CoaB
39 identified two inhibitors with different chemical scaffolds. Hit expansion led to the
40 discovery of potent inhibitors of *M. tuberculosis* CoaB. Crucially we further show that
41 these compounds bind to a novel cryptic allosteric site within CoaB.

42

43

44

45

46

47

48

49

50

51

52

53

54 **Introduction**

55 Tuberculosis (TB) is the most prevalent and deadly infectious disease worldwide and
56 remains a global epidemic. Despite the availability of treatment, this disease caused, by
57 *Mycobacterium tuberculosis*, still claims 1.5 million lives each year¹. Current treatment
58 regimens are long which presents an obstacle for patient adherence and imposes a heavy
59 social and economic burden on countries with a high incidence of TB. It is therefore
60 critical to explore novel targets and find new and more effective drugs to combat this
61 disease.

62 Coenzyme A (CoA) is an essential and ubiquitous cofactor, involved in numerous
63 metabolic pathways with a large number of different enzymes requiring it for activity².
64 CoA is essential for the synthesis of phospholipids, fatty acids, polyketides, and non-
65 ribosomal peptides, for the operation of the tricarboxylic acid cycle and in the degradation
66 of lipids³. The importance of CoA for essential post-translational modifications of
67 proteins is also well established in both eukaryotes and prokaryotes with various proteins
68 post-translationally modified by thioester derivatives of CoA (acylation) or CoA itself
69 (phosphopantetheinylation and CoAlation), while several other post-translational
70 modifications depend indirectly on CoA through the mevalonate pathway⁴⁻⁷.
71 Furthermore, dephospho-CoA, an intermediate of the CoA pathway, is incorporated into
72 some RNA transcripts during transcription initiation thereby serving as a non-canonical
73 transcription initiating nucleotide⁸. These RNA modifications have functional
74 consequences and occur in both eukaryotes and bacteria⁸. In *M. tuberculosis*, CoA plays
75 a pivotal role in the biosynthesis of complex lipids that are crucial components of the cell
76 wall and required for pathogenicity⁹. It is also needed for the degradation of lipids,
77 including cholesterol, which are the primary source of energy for this organism during
78 infection^{10,11}. The CoA pathway is therefore an attractive pathway for drug discovery for

79 many different infectious diseases, including TB, given its ubiquitous nature, wide
80 metabolic and functional impact of its inhibition and lack of sequence conservation
81 between prokaryotes and humans.

82 The biosynthesis of CoA from pantothenic acid (vitamin B₅) is performed in five steps,
83 sequentially catalysed by the enzymes pantothenate kinase (CoaA, also known as PanK),
84 phosphopantothenoylcysteine synthetase (CoaB), phosphopantothenoylcysteine
85 decarboxylase (CoaC), phosphopantetheine adenylyltransferase (CoaD) and dephospho-
86 CoA kinase (CoaE). However, in the vast majority of prokaryotes, including *M.*
87 *tuberculosis*, CoaB and CoaC are encoded by a single gene to produce a fused
88 bifunctional enzyme (CoaBC). Transcriptional silencing of individual genes of the CoA
89 biosynthesis pathway of this pathogen identified CoaBC as uniquely bactericidal within
90 the CoA pathway, highlighting it as a good candidate for drug discovery¹².

91 CoaBC comprises two enzymes in a single polypeptide chain and converts 4'-
92 phosphopantothenate to 4'-phosphopantetheine in three steps. First, 4'-
93 phosphopantothenate (PPA) reacts with CTP to form 4'-phosphopantothenoyl-CMP with
94 the release of pyrophosphate. This intermediate subsequently reacts with cysteine to form
95 4'-phosphopantothenoylcysteine (PPC) with the release of CMP with these two steps
96 being catalysed by CoaB. The product of CoaB is then decarboxylated by CoaC to 4'-
97 phosphopantetheine an enzyme of the homo-oligomeric flavin-containing decarboxylase
98 (HFCD) protein family. X-ray crystal structures have been reported for the individual
99 CoaB and CoaC enzymes in several organisms, including a structure of CoaB from
100 *Mycobacterium smegmatis*, a close relative of *M. tuberculosis* However, a structure of
101 the full-length bifunctional CoaBC was missing.

102 Here we report the structure of the bifunctional CoaBC of *M. smegmatis* at 2.5 Å. We
103 identify a previously unknown allosteric site in CoaB and crucially, we report the

104 identification of the first *M. tuberculosis* CoaBC allosteric inhibitors. Using X-ray
105 crystallography and enzyme kinetic experiments, we define the mode of binding of one
106 of the inhibitors and show its impact on the protein structure and function. These results
107 further illustrate the potential of CoaBC as a novel drug target in *M. tuberculosis*.

108

109 **Results**

110 **Overall structure of CoaBC**

111 Because the HFCD protein family of flavin-binding proteins are known to form homo-
112 oligomers¹³, we performed native electrospray-ionization mass spectrometry (ESI-MS)
113 to investigate the stoichiometry of CoaBC, previously proposed to form a dodecamer¹³.
114 Both *M. tuberculosis* CoaBC (MtbCoaBC) (Figure S1A) and *M. smegmatis* CoaBC
115 (MsmCoaBC) (Figure S1B) exclusively exhibited a dodecameric assembly, with no other
116 oligomeric species observed in the spectra, consistent with a strong interaction between
117 the subunits of the complex. The dodecamer of MtbCoaBC was centred around the 56+
118 charge state, with an observed mass of 537 kDa, while the dodecamer of MsmCoaBC was
119 centred around the 52+ charge state, with an observed mass of 523 kDa. These masses
120 are 1-2% higher than the expected masses of 525 and 518 kDa for MtbCoaBC and
121 MsmCoaBC respectively, which can be attributed to the non-specific binding of solvent
122 molecules or ions to the protein complexes under the soft ionization conditions employed.
123 Structures of a few proteins of the HFCD family have been determined¹⁴⁻¹⁸. All of these
124 structures show either a homo-trimeric or homo-dodecameric arrangement of the flavin-
125 containing Rossmann-fold with trimers forming at each of the vertices of the tetrahedron
126 in the case of a dodecameric arrangement¹⁵. However, all of these proteins, unlike
127 CoaBC, contain only a single functional domain. We solved the structure of MsmCoaBC
128 at 2.5 Å resolution (Figure 1A), in the presence of CTP and FMN (Figure 1B, S2A and

129 S2B), using crystals belonging to the H3₂ space group with an asymmetric unit containing
130 four protomers forming two CoaBC dimers. Data collection and refinement statistics are
131 summarized in (Table S1). The final model (residues 2-412) covers both CoaC and CoaB,
132 but densities for several residues in three loop regions in CoaB are not observed (residues
133 290-298, 336-342, 363-376). However, all these residues except for 375 and 376 can be
134 seen the MsmCoaB X-ray crystal structure (PDB: 6TH2) that we also solved in this work
135 at 1.8 Å. The N-terminal CoaC of MsmCoaBC (residues 1-179) forms the same type of
136 dodecameric arrangement seen in other HFCD family proteins such as the peptidyl-
137 cysteine decarboxylase EpiD¹⁵ and sits at the core of the dodecamer (Figure 1A and 1C).
138 The active site of CoaC sits at the interface between two protomers of the CoaC trimer
139 and a protomer of an adjacent CoaC trimer with the FMN site facing inwards towards the
140 hollow centre of the dodecamer (Figure 2A). A flexible flap that was observed before
141 covering a reaction intermediate bound to *Arabidopsis thaliana* CoaC¹⁹ is also observed
142 in some of the protomers, but in an open conformation (Figure 1B).
143 CoaC and CoaB are connected through a small loop region (residues 180-189) that tightly
144 interacts with both enzymes. CoaB also displays a Rossmann fold consistent with the
145 several other CoaB structures solved previously, including both the eukaryotic form, in
146 which CoaB exists as an individual polypeptide, and the bacterial form where CoaB is
147 typically fused with CoaC²⁰⁻²². Each CoaB of MsmCoaBC (residues 190-414) dimerises
148 with a CoaB belonging to an adjacent trimer (Figure 1C). The full protein resembles a
149 tetrahedron with CoaB dimers positioned at the six edges and CoaC trimers at the four
150 vertices (Figure 1A).
151 The shortest distance between a pair of CoaB and CoaC active sites is ~30 Å (Figure 2B).
152 Nevertheless, a flexible loop (residues 362-377) that covers the 4'-phosphopantothenate
153 site when this substrate binds to the enzyme²⁰ can be seen in our MsmCoaB structure

154 away from the active site. A superposition of our MsmCoaB dimer structure with
155 MsmCoaBC shows the loop extending towards the CoaC active site (Figure 2B). This
156 long loop (15-16 amino acids) is present in all CoaBCs (Figure S3) and it is possible that
157 it helps channel the substrate from the CoaB to the CoaC active site.

158 The small differences (RMSD = 1.147) in overall structure of CoaB dimers in the full
159 length MsmCoaBC and the MsmCoaB crystal structure solved at 1.8 Å (PDB: 6TH2) can
160 be attributed to artefacts of crystal packing (Figure S4). Similarly, the CoaC structure
161 does not seem to differ between full length MsmCoaBC and the available individual CoaC
162 structures. However, when MsmCoaB (residues 186-414) is expressed alone, the protein
163 does not dimerise in solution and is inactive (not shown). This contrasts with *E. coli*
164 CoaB, which still dimerises and is functional when expressed on its own without the N-
165 terminal CoaC^{23,24}. The CoaB dimer interface is mostly conserved, but there are clear
166 differences in the dimerisation region between MsmCoaB and *E. coli* CoaB that could
167 help to explain the different observed behaviours (Figure S3). The absence of
168 dimerization for the MsmCoaB when expressed alone suggests that the interactions
169 between CoaC and CoaB in *M. smegmatis*, and likely all other *Mycobacteriaceae*, are
170 fundamental for CoaB dimerisation and activity. This idea is reinforced by the fact that
171 the residues located at the interface of the two enzymes (CoaB and CoaC) are well
172 conserved in all *Mycobacteriaceae* and somewhat conserved in the sub-order
173 *Corynebacterineae* but not outside of this group (Figure S3).

174 The CoaB dimerisation region forms a β -sandwich composed of eight anti-parallel β -
175 strands, related by 2-fold symmetry, that contacts with the active site (Figure 2C and 2D).
176 Comparison of the MsmCoaB with human CoaB reveals that the human and many other
177 eukaryotic CoaBs²¹ possess two extra α -helices and β -strands involved in the
178 dimerisation interface that help stabilise the dimer in the absence of CoaC (Figure S5).

179 The CoaB active site is enclosed by a loop that extends from the opposing protomer and
180 is observed for the first time in this work. This loop contains a motif “K-X-K-K”, which
181 is widely conserved in bacteria (Figure S3), with few exceptions, and each lysine either
182 interacts directly with the triphosphate group of CTP or through highly coordinated
183 waters (Figure 2C). Also observed for the first time is the coordination of a cation by the
184 triphosphate group and D281 (Figure 2C and S6). While magnesium or manganese are
185 the favoured cations for CoaB activity ²⁵, calcium is observed in our structures instead,
186 due to the high concentration present in the crystallization condition.

187

188 **CoaBC is regulated by CoA thioesters**

189 It is known that CoA biosynthesis is regulated, in many organisms, at the first step of the
190 pathway, catalysed by the enzyme CoaA ³. *M. tuberculosis* and many other mycobacteria
191 possess two isoforms of this enzyme (type I and III), however only the type I isoform
192 seems to be active based on studies in *M. tuberculosis* ²⁶. CoA and its thioesters
193 competitively inhibit this enzyme by binding to the ATP site with CoA being the strongest
194 regulator ^{27,28}. Nevertheless, at physiologically relevant levels of CoA there is only a low
195 level inhibition of CoaA ²⁸. It is also known that CoaD, the enzyme that catalyses the
196 fourth step of the pathway, is competitively inhibited by CoA and its product dephospho-
197 CoA ^{29,30}. However, nothing was known about the regulation of CoaBC. We therefore
198 examined the effect of CoA and several of its thioesters (acetyl-CoA, malonyl-CoA and
199 succinyl-CoA) on MtbCoaBC activity, using a coupled enzymatic assay that quantifies
200 the release of pyrophosphate (EnzCheck pyrophosphate assay). Potent regulation of
201 CoaB activity by CoA and acyl-CoAs was observed, with IC₅₀ values ranging from 38 to
202 148 μ M, far below the predicted intracellular concentrations of acyl-CoAs ³¹, with
203 succinyl-CoA displaying the highest inhibition (Figure 3A and Table 1). Competition

204 assays with the three substrates and acetyl-CoA show a competitive mode of inhibition
205 relative to CTP and PPA, and non-competitive inhibition for L-cysteine (Figure 3B). In
206 the absence of a crystal structure to confirm the mode of binding, these results suggest
207 that acyl-CoAs most likely bind to the active site itself, competing directly with CTP and
208 PPA. Interestingly both acyl-CoAs, involved in fatty acid synthesis, as well as those,
209 involved in the TCA cycle, show inhibition of CoaB with larger fatty acyl chains showing
210 higher inhibition of CoaB.

211

212 **Identification of CoaB inhibitors using high-throughput screening**

213 Although the CoA biosynthetic pathway is considered an attractive target for drug
214 discovery, CoA pathway inhibitors displaying potent whole cell activity are relatively
215 rare. Few CoaBC inhibitors have been reported to date and these are in majority substrate
216 mimicking^{24,32}.

217 In order to identify novel MtbCoaBC inhibitors, we conducted a high-throughput screen of
218 215,000 small molecules targeting CoaB activity. To do this an end-point pyrophosphate
219 quantification assay was used (Biomol Green). The most potent hits identified were
220 compounds **1a** and **2a** with IC₅₀ values of 9 and 3.1 μM respectively (Table S2),
221 originating from two different chemical series. A search was then performed for
222 commercially available analogues. Testing of analogues of the initial hits resulted in the
223 identification of more potent compounds with sub-micromolar IC₅₀ values (Table 1,
224 Figure 4A, Table S2 and Figure S7). Of these, compounds **1b** and **2b** (Figure 4A and
225 Table 1) with IC₅₀ values of 0.28 and 0.08 μM respectively were identified as the most
226 potent of the two chemical series and therefore were selected for further work.

227

228 **Elucidation of the mode of inhibition**

229 Following the identification of potent MtbCoaB inhibitors we went on to determine their
230 mode of inhibition using kinetic assays. For this, the EnzCheck coupled enzyme assay
231 that measures the release of pyrophosphate was used. Control experiments were first
232 performed to assess compound activity against the two coupling enzymes and the
233 compounds were found to be inactive at 100 μ M. The IC₅₀ values for the compounds
234 against CoaB were reassessed with this assay and the values obtained were in line with
235 the primary screening assay (Table S2).

236 Competition experiments were then performed using the three CoaB substrates for the
237 two most potent compounds of each chemical series (**1b** and **2b**). Compound **1b** was
238 found to preferentially bind to the enzyme-substrate complex with uncompetitive
239 inhibition observed for all substrates (Figure 4B), consistent with the compound binding
240 preferentially when the three substrates are bound. Compound **2b** shows mixed inhibition
241 relative to CTP and uncompetitive inhibition for L-cysteine and PPA (Figure 4C). It is
242 known that CoaB forms the phosphopantothienoyl-CMP intermediate in the absence of L-
243 cysteine³³ and it is likely, due to spatial constraints, that cysteine can only bind at the
244 active site after the release of pyrophosphate. The data is therefore consistent with
245 compound **1b** preferentially binding after L-cysteine enters the active site, for to the last
246 step of catalysis and the formation of 4'-phosphopantothienoylcysteine and CMP.
247 However, compound **2b** shows a mixed inhibition for CTP, reflecting a slightly different
248 mechanism of action. These results obtained for both compounds suggest the existence
249 of an allosteric site in the CoaB moiety of MtbCoaBC.

250

251 **Structural basis for inhibition of CoaB by allosteric inhibitors**

252 In order to elucidate the binding mode of compound **1b** we used a truncation of the
253 MsmCoaB (residues 187-414) that was previously crystallized before by others in the

254 presence of CTP (PDB code: 4QJI) at 2.65 Å resolution. The screening for new
255 crystallization conditions allowed us to find a new CTP containing condition that gave
256 excellent resolution (~1.8 Å). Comparison of this structure with the full length
257 MsmCoaBC showed only minor differences that can be attributed to crystal packing
258 (Figure S4). Hence this crystallization system could be used to validate CoaB inhibitors
259 binding outside of the CTP site.

260 MsmCoaB was co-crystallized with CTP in the absence of compound **1b** and overnight
261 soaking of the crystals with this compound was performed. A Co-crystal structure of
262 MsmCoaB with compound **1b** was obtained and showed that the compound was bound
263 to a site at the dimer interface of CoaB, in a deep cavity that is occluded when the
264 compound is absent (Figure 5A-B and S8). Each CoaB dimer contains two of these sites,
265 which are formed by a sandwich of eight β-strands and a long loop that contains the
266 conserved “K-X-K-K” motif. This site opens to the active site and the inhibitor also
267 contacts with D281 that is involved in the coordination of the cation (Figure 5C). The
268 opening/closing of this cryptic allosteric site is mediated by the side chain of R207 of the
269 opposing protomer (Figure 5D) that moves 5.5 Å at the furthest point and to a smaller
270 extent by the side chain of F282 that moves 2 Å. R207 has previously been shown to be
271 critical for the second half of the reaction catalysed by CoaB, the conversion of the 4'-
272 phosphopantothenoyl-CMP intermediate to PPC, with almost no conversion of the
273 intermediate to PPC detected when this arginine is mutated to glutamine³³. Given the
274 position of this arginine it is likely that it is involved in the binding of cysteine. Despite
275 the absence of a crystal structure with cysteine, kinetic data showing uncompetitive
276 inhibition with cysteine is consistent with this.

277 This allosteric site is comprised of a large group of hydrophobic residues (I209, F282
278 L304 of protomer A and L203, I292, P299 and I302 of protomer B) many of which form

279 hydrophobic interactions with compound **1b** (Figure 5C). Several π -interactions between
280 the compound and the protein are also observed and involve D281 and F282 of protomer
281 A and R207 of protomer B (Figure 5D). Hydrogen-bond interactions are formed with
282 D281 and F282 of protomer A and R207 of protomer B. Water-mediated interactions are
283 also observed for a group of residues that sit at the outer edge of the site (L203, H286 and
284 D303) that is formed exclusively by protomer B (Figure 5C).

285 We propose that upon binding of L-cysteine, the R207 side chain moves towards the
286 active site, and is likely involved in stabilizing/orienting L-cysteine to attack the
287 phosphopantothenoyl-CMP intermediate. This movement opens the allosteric site, which
288 allows binding of allosteric inhibitors to the newly created cavity. The allosteric inhibitors
289 will then stabilize the enzyme in its substrate bound state with the position of R207
290 becoming locked by several hydrogen-bonds with the side chain of D281 of protomer A,
291 the backbone carbonyl group of I292 and the side chain of D204 of protomer B but also
292 by the π -interactions with the compound (Figure 5C). The residues around this site and
293 crucially R207 are conserved across many microorganisms, suggesting that this allosteric
294 site is present in most, if not all bacterial CoaBCs (Figure S3 and S9A). Interestingly,
295 even though overall sequence identity is very low between the human CoaB and
296 MsmCoaB (22%), the human enzyme also contains an arginine equivalent to R207 and a
297 roughly similar interface with several conserved residues, but there are stark differences
298 in the relative position of the residues at this site between the two enzymes (Figure S9B).
299 While we were not able to obtain co-crystal structures with other inhibitors, *in silico*
300 docking helped to provide a possible explanation for the structure-activity relationship
301 observed for series one and two. The highest-scoring docking pose of compound **1b** the
302 most potent inhibitor of series one, was almost identical to that observed in the co-crystal
303 structure (Figure S10A), and the analogues for which docking was performed adopted a

304 similar binding pose. The lower activity of compound **1a** relative to compound **1b** could
305 be explained by the loss of water-mediated hydrogen bonds (Figure 5C, S10B), while the
306 lower activity of compound **1c** could be explained by the loss of the carbonyl group which
307 faces a highly electropositive area of the protein (Figure S10C). Compound **2b** is
308 predicted to form direct hydrogen bonds at the bottom of the allosteric site, similar to
309 those formed by compound **1b** but also to interact directly with L203 and H286, forming
310 extra hydrogen bonds at the top of the allosteric site (Figure 6). For compound **1b** the
311 interactions at the top of the site are water mediated (Figure 5C). This could explain the
312 higher potency of compound **2b**. Compounds **2c** and **2d** are also predicted to form direct
313 hydrogen bond interactions at the top of the allosteric site, but the interactions at the
314 bottom of the site are not as favourable due to the presence of extra hydroxyl groups
315 (Figure S10D-F). The remaining compounds in series two, which have fewer hydroxyl
316 groups and/or with hydroxyl groups in different positions, lose the ability to form
317 hydrogen bonds, consistent with the weaker inhibitory effect observed (Table S2).

318

319 **Screening of CoaBC inhibitors against *M. tuberculosis***

320 The in vitro whole cell activity of the compounds was further evaluated by their ability
321 to inhibit *M. tuberculosis* growth on different carbon sources. None of the compounds
322 exhibited activity in media containing glycerol or cholesterol as the main carbon source.
323 We then tested whether the lack of inhibitory activity could be attributed to the presence
324 of BSA by determining the whole cell activity of the three most potent inhibitors against
325 *M. tuberculosis* in GAST/Fe minimal media. All the tested compounds exhibited
326 moderate to low activity in this media with compound **2b** displaying the best activity of
327 the three (Table 2). The observed differences in potency between the enzymatic assay and

328 whole cell activity are likely related to low compound permeation, high efflux or
329 metabolisation.

330

331 **Discussion**

332 CoA is an essential co-factor ubiquitous in all domains of life. For many years, this
333 pathway has been considered an attractive drug target to develop new antibiotics against
334 a wide range of pathogens including *M. tuberculosis*. Furthermore, the recent
335 identification of CoaBC as a key fragility point in the CoA pathway of this organism ¹²,
336 combined with the extremely low sequence identity with the human CoaB (25%) makes
337 this enzyme an highly attractive drug discovery target.

338 However, we were aware that the many questions remaining at the start of this work about
339 the organization and regulation of this bi-functional enzyme could have significant
340 implications for drug discovery. We therefore set out to obtain a full-length structure of
341 a CoaBC from mycobacteria and we were successful in solving the full length
342 MsmCoaBC but also MsmCoaB alone, which share very high sequence identity with the
343 *M. tuberculosis* orthologue (86% full-length, 84% CoaB enzyme) and hence valuable
344 tools for studying *M. tuberculosis* CoaBC. The CoaBC organization we revealed is
345 similar to other HFCD family proteins ¹⁵ but unique in the sense that it contains more than
346 one domain and highlights how the arrangement of the fused enzymes is essential for
347 mycobacterial CoaB dimerisation and function.

348 Regulation of the CoA biosynthesis pathway by its product (CoA) was known to occur
349 for other enzymes of the pathway but no information was available for CoaBC. We
350 demonstrate that both CoA as well as several CoA thioesters regulate CoaBC by
351 inhibiting CoaB activity with succinyl-CoA showing the greatest inhibition of the tested
352 acyl-CoAs, and that these molecules act in a competitive manner with CTP and PPA and

353 a non-competitive manner with L-cysteine. This is consistent with these molecules
354 binding to the CoaB active site but not to the L-cysteine sub-site.
355 CoA and acyl-CoAs inhibit both CoaA and CoaD enzymes to varying extents ^{28,30,34}.
356 However, the inhibitory effect of CoA and its thioesters in their activity is low when
357 compared to what we observed in CoaBC and consequently the impact of the intracellular
358 level of these molecules will be higher in CoaBC . We therefore report a new and
359 important mechanism of regulation of de novo CoA biosynthesis, mediated by the action
360 of CoA thioesters on CoaBC. Since the reported intracellular levels of these molecules
361 are normally above the observed IC₅₀ the activity of CoaBC is highly inhibited. This
362 correlates well with previous work showing that “de novo” CoA biosynthesis closely
363 matches dilution due to cell division ³⁵.
364 Although the CoA pathway and CoaBC have been the subject of many drug discovery
365 efforts, few non-substrate-mimicking inhibitors of CoaBC have been reported ²⁴. Our
366 work identifies two related chemical scaffolds that potently inhibit the activity of the
367 CoaB moiety of MtbCoaBC through a new cryptic allosteric site that sits in the dimer
368 interface region of the CoaB enzyme. This site is closed in the CTP-bound structure, by
369 the side chain of R207 a residue known to be involved in the second and final step of the
370 reaction catalysed by CoaB – the conversion of the 4'-phosphopantothenoil-CMP
371 intermediate to PPC ³³. Considering the role of this in the final step of product formation
372 and that compound **1b** shows uncompetitive inhibition relative to all CoaB substrates, we
373 propose that the opening of this site occurs upon binding of the final substrate L-cysteine.
374 Currently it is not clear whether this new allosteric site is exploited by a natural ligand,
375 as we were unable to identify such a biomolecule. Nevertheless, the conservation of
376 residues at this site, across a variety of bacteria, indicates that this feature might be
377 common to many, if not all, bacterial CoaBs.

378 Drug discovery against *M. tuberculosis* is rich in examples of compounds with potent
379 activity against an essential enzyme but with a complete lack of whole cell activity due
380 to the impermeable cell wall of this organism, efflux pumps, target modification enzymes
381 and extensive capacity to metabolise compounds³⁶. The lack of in vitro whole cell activity
382 displayed by the CoaB inhibitors reported in this work, may relate to any of these issues.
383 However, the activity observed in albumin free media (GAST media) also points to the
384 possibility of compound binding to albumin interfering with the assay. Nevertheless, the
385 promising biochemical and structural data described herein further validates CoaBC as a
386 promising novel anti-tubercular drug target by showing a new allosteric site that can be
387 targeted by potent inhibitors.

388

389 **Materials and methods**

390 **Cloning and protein purification**

391 *Mycobacterium tuberculosis* and *Mycobacterium smegmatis* *coaBC* genes were amplified
392 from genomic DNA of *M. tuberculosis* H37Rv strain, obtained from ATCC
393 (ATCC25618D-2) and genomic DNA of *M. smegmatis* mc² 155 (graciously provided by
394 Dr. Nuno Empadinhas), and cloned into a pET28a vector (Novagen), modified to include
395 an N-terminal 6xHis-SUMO tag. *M. smegmatis* *coaB* construct was obtained from Seattle
396 Structure Genomics Center for Infectious Disease. The same protein purification protocol
397 was used for both *M. tuberculosis* and *M. smegmatis* CoaBC constructs.

398 *E. coli* BL21(DE3) containing pET28aSUMO-CoaBC was grown in 2XYT media at 37
399 °C until an O.D.₆₀₀ = 0.6. IPTG was then added to a final concentration of 0.5 mM at the
400 temperature changed to 18 °C for 18-20h. Cells were then harvested by centrifugation, re-
401 suspended in 50 mM TRIS pH 8.0, 250 mM NaCl, 20% (w/v) glycerol, 20 mM imidazole,
402 5 mM MgCl₂ with protease inhibitors tablets (Roche) and DNaseI (Sigma). Cells were

403 lysed with an Emulsiflex (Avestin) and the resultant cell lysate was centrifuged at 27000
404 x g for 30 min to remove cell debris. Recombinant CoaBCs were purified with a HiTrap
405 IMAC Sepharose FF column (GE-Healthcare), equilibrated with 50 mM TRIS pH 8.0,
406 250 mM NaCl, 20% glycerol (w/v) and 20mM Imidazole. Elution was performed in the
407 same buffer with 500mM Imidazole. Protein was dialysed in 25 mM TRIS pH 8 and 150
408 mM and SUMO tag was cleaved overnight at 4 °C by adding Ulp1 Protease at 1:100
409 ratio. CoaBC was concentrated and loaded in a Superdex 200 column equilibrated with
410 25mM TRIS pH 8.0, 150 mM NaCl. Fraction purity was determined by SDS-page and
411 the purest fractions were pooled, concentrated to ~10 mg.ml⁻¹ for *M. tuberculosis* CoaBC
412 and 30 mg.ml⁻¹ for *M. smegmatis* CoaBC, flash frozen in liquid nitrogen and stored at -
413 80 °C.

414 *E. coli* BL21(DE3) containing the *M. smegmatis* CoaB construct with a N-terminal non-
415 -cleavable 6xhis tag was grown and harvested as above and re-suspended in 20 mM
416 HEPES pH 7.0, 500 mM NaCl, 20 mM imidazole, 5 mM MgCl₂ with protease inhibitors
417 tablets (Roche) and DNaseI (Sigma). Cells were lysed with an Emulsiflex (Avestin) and
418 cell lysate was centrifuged at 27000 g for 30 mins to remove cell debris. Recombinat *M.*
419 *smegmatis* CoaB was purified with a HiTrap IMAC Sepharose FF column (GE-
420 Healthcare), equilibrated with 20 mM HEPES pH 7.0, 500 mM NaCl and 20 mM
421 imidazole. Elution was carried in the same buffer with 500 mM imidazole. Protein was
422 concentrated and loaded on a Superdex 200 column equilibrated with 20mM HEPES pH
423 7.0 and 500 mM NaCl. Fraction purity was assessed by SDS-page and the purest fractions
424 were pooled concentrated to 22 mg. ml⁻¹, flash frozen in liquid nitrogen and stored at -80
425 °C.

426

427 **Native mass spectrometry**

428 Spectra were recorded on a Synapt HDMS mass spectrometer (Waters) modified for
429 studying high masses. MtCoaBC and MsCoaBC were exchanged into NH₄OAc (500 mM,
430 pH 7.0) solution using Micro Bio-Spin 6 chromatography columns (Bio-Rad). 2.5 µL of
431 sample solution was injected into a borosilicate emitter (Thermo Scientific) for sampling.
432 Instrument conditions were optimized to enhance ion desolvation while minimizing
433 dissociation of macromolecular complexes. Typical conditions were capillary voltage
434 1.8–2.0 kV, sample cone voltage 100 V, extractor cone voltage 1 V, trap collision voltage
435 60 V, transfer collision voltage 60 V, source temperature 20 °C, backing pressure 5 mbar,
436 trap pressure $3\text{--}4 \times 10^{-2}$ mbar, IMS (N₂) pressure $5\text{--}6 \times 10^{-1}$ mbar and TOF pressure 7--
437 8×10^{-7} mbar. Spectra were calibrated externally using cesium iodide. Data acquisition
438 and processing were performed using MassLynx 4.1 (Waters).

439

440 **Crystallization**

441 For both full length *M. smegmatis* CoaBC and CoaB alone, the crystallization screens and
442 optimization were performed at 18 °C using the sitting-drop vapour diffusion method. For
443 CoaBC 300 nL of pure protein at 30 mg.ml⁻¹, pre-incubated with 3 mM CTP and 10 mM
444 MgCl₂, was mixed in 1:1 and 1:2 (protein to reservoir) ratio with well solution using a
445 mosquito robot (TTP labtech). Initial conditions were obtained in the Classics lite
446 crystallization screen (Qiagen), solution 1. Crystals obtained in this condition diffracted
447 poorly, therefore several rounds of optimization were performed. The final optimised
448 condition consisted of 0.1 M BisTris pH 6.5, 10 mM CoCl₂ 0.8 M 1,6-hexanediol.
449 Crystals appeared after three days in both conditions. A cryogenic solution was prepared
450 by adding ethylene glycol up to 30% (v/v) to mother liquor. Crystals were briefly
451 transferred to this solution, flash frozen in liquid nitrogen and stored for data collection.

452 For MsmCoaB 200 nL of pure protein at 22-24 mg.mL⁻¹ with 10 mM CTP was mixed in
453 1:1 ratio with well solution using a Phoenix robot (Art Robbins). Crystals were obtained
454 in Wizards classics III&IV (Rigaku) solution G4 consisting of 20% (w/v) PEG 8000,
455 0.1M MES pH 6.0 and 0.2 M calcium acetate. Crystals appeared after 2 days.

456 To obtain ligand-bound structures, soaking was performed condition using the hanging-
457 drop vapour-diffusion method as follows: 2 uL of a solution containing 20% (w/v) PEG
458 8000, 0.1M MES pH 6.0, 0.2 M calcium acetate, 0.25 M NaCl 10% (v/v) DMSO and 1-
459 5 mM inhibitors was left to equilibrate against 500 µl of reservoir solution for 3 days.
460 Crystals were then transferred to the pre-equilibrated drops and incubated for 24h. A
461 cryogenic solution was prepared by adding 2-Methyl-2,4-pentanediol up to 25% (v/v) to
462 mother liquor. Crystals were briefly transferred to this solution, flash frozen in liquid
463 nitrogen and stored for data collection.

464 While we have also obtained *M. tuberculosis* CoaBC crystals they did not diffract and
465 our optimization efforts failed to improve them.

466

467 **Data collection and processing**

468 The data sets were collected at stations I02 and I03 at Diamond Light Source (Oxford,
469 UK). The diffraction images were processed with AutoPROC³⁷ using XDS³⁸ for
470 indexing and integration with AIMLESS³⁹ and TRUNCATE⁴⁰ from CCP4 Suite⁴¹ for
471 data reduction, scaling and calculation of structure factor amplitudes and intensity
472 statistics.

473

474 **Structure solution and refinement**

475 MsmCoaB and MsmCoaBC structures were solved by molecular replacement using
476 PHASER⁴² from the PHENIX software package⁴³. For MsmCoaB the atomic

477 coordinates of MsmCoaB structure (PDB entry 4QJI) were used as a search model.
478 Ligand bound structures were solved using our highest resolution MsmCoaB apo form
479 structure (PDB entry 6TH2). For MsmCoaBC atomic coordinates of *Arabidopsis thaliana*
480 CoaC (PDB entry 1MVL)¹⁹ and our highest resolution CoaB structure (PDB entry 6TH2)
481 were used as search models. Model building was done with Coot⁴⁴ and refinement was
482 performed in PHENIX⁴³. Structure validation was performed using Coot and PHENIX
483 tools^{43,44}. All figures were prepared using Pymol (The PyMOL Molecular Graphics
484 System, Version 2.0 Schrödinger, LLC.) and ligand interactions calculated with Arpeggio
485⁴⁵.

486

487 **High-throughput screening**

488 Potential inhibitors of CoaBC were assessed at room temperature using a PHERAStar
489 microplate reader (BMG Labtech). Pyrophosphate produced by CoaB was converted to
490 two molecules of inorganic phosphate using a pyrophosphatase. Phosphate was then
491 detected using the BIOMOL® Green reagent (Enzo Life Sciences), which when bound
492 to phosphate absorbs light at 650 nm. An end-point assay was carried out in clear, flat-
493 bottom, polystyrene, 384-well plates (Greiner) in an 50 µl reaction volume containing
494 100 mM TRIS, pH 7.6; 1 mM MgCl₂; 1 mM TCEP; 0.03 U/mL pyrophosphatase; 2 µM
495 CTP; 40 µM L-cysteine; 30 µM PPA and 30 nM MtbCoaBC. Assays were performed by
496 adding 25 µL of a 2-times concentrated reaction mixture containing all components with
497 the exception of the enzymes to all wells, and the reactions started by adding 25 µL of a
498 2-times concentrated enzyme mixture. The reaction was carried out for 2 h at room
499 temperature, before 50 µL of BIOMOL® Green reagent was added and incubated for a
500 further 20 min prior to reading.

501

502 **Inorganic pyrophosphatase-purine nucleoside phosphorylase PNP-PPIase assay.**

503 The commercially available EnzCheck pyrophosphate assay kit (E-6645) (Life
504 Technologies) was used for this assay. The final reaction composition used was 0.03
505 U/mL inorganic pyrophosphatase, 1 U/mL purine nucleoside phosphorylase, 1 mM
506 MgCl₂, 200 μM MESG, 100 mM TRIS pH 7.5, 1 mM TCEP, 32 nM MtbCoaBC, 125
507 μM CTP, 125 μM PPA, 500 μM L-cysteine, and various concentrations of compounds
508 being tested for inhibition all prepared from DMSO stock solutions (compounds of series
509 one and two) or water (CoA and CoA thioesters). Assays were performed on either a
510 CLARIOStar or PHERAStar microplate reader (BMG Labtech) in 96-well plates
511 (Greiner). A substrate mixture containing the substrates and the inhibitor was pre-
512 incubated at 25 °C for 10 min. An enzyme solution was prepared and separately pre-
513 incubated at 25 °C for 10 min. The reaction was initiated by the addition of the substrates
514 to the solution containing the enzyme to a final volume of 75 μL. Enzymatic activity was
515 monitored by following the absorbance at 360 nm for 30 min (100 cycles/20 s each cycle).
516 Assays were performed in triplicates, including a negative control (lacking PPA) and a
517 positive control (lacking inhibitor).

518 Competition assays were performed using the same conditions but with variable substrate
519 concentrations (31.25 μM, 62.5 μM, 125 μM, 250 μM and 500 μM for CTP and PPA,
520 31.25 μM, 62.5 μM, 93.75 μM 125 μM and 250 μM for L-cysteine).

521

522 ***M. tuberculosis* strains and growth conditions**

523 MIC determination for *M. tuberculosis* H37RvMA was performed as previously
524 described⁴⁶ in the following media: 7H9/ADC/glycerol (4.7 g/L Difco Middlebrook 7H9
525 base, 100mL/L Middlebrook albumin (BSA)-dextrose-catalase (ADC) Difco
526 Middlebrook, 0.2% glycerol and 0.05% Tween-80), 7H9/Cholesterol/Tyloxapol (4.7 g/L

527 7H9 base, 0.81 g/L NaCl, 24 mg/L cholesterol, 5 g/L BSA fraction V and 0.05%
528 Tyloxapol), GAST/Fe (0.3 g/L of Bacto Casitone (Difco), 4.0/L g of dibasic potassium
529 phosphate, 2.0 g/L of citric acid, 1.0 g/L of L-alanine, 1.2 g/L of magnesium chloride
530 hexahydrate, 0.6 g/L of potassium sulfate, 2.0 g/L of ammonium chloride, 1.80 ml/L of
531 10 N sodium hydroxide, 10.0 ml of glycerol 0.05% Tween 80 and 0.05 g of ferric
532 ammonium citrate adjusted to pH 6.6.

533

534

535

536

537

538

539

540

541

542

543

544

545

546

547

548

549

550

551

552

553

554 **Figure Legends**

555 **Figure 1: X-ray crystal structure of FMN and CTP bound MsmCoaBC.**

556 (A) Full aspect of the dodecameric CoaBC with CoaC represented in teal and CoaB in
557 gold. (B) View of a CoaBC dimer with FMN and CTP shown. Each protomer is coloured
558 differently. The CoaC active site flexible flap is highlighted in blue. (C) In the left panel,
559 a CoaBC trimer is shown with the CoaC coloured in teal and CoaB in gold. On the right
560 panel dimerization of two CoaBC trimers is shown with CoaC coloured in teal or grey for
561 different trimers. Each CoaB forms a dimer with protomers from different trimers.

562

563 **Figure 2: Detailed view of MsmCoaBC active sites and MsmCoaB dimerisation** 564 **interface.**

565 (A) View of CoaC active site with FMN bound. The active site sits between two
566 protomers of one trimer (gold and red) and a third protomer from an adjacent trimer
567 (green). Hydrogen bonds are depicted in yellow and π -interactions are in blue. (B)
568 Superposition of a CoaB crystal structure (PDB code: 6TH2) in green, with full length
569 CoaBC (teal) showing the active site flaps (brown) of the CoaB and CoaC enzymes. (C)
570 Detailed view of the CTP binding site. Cartoon and residues belonging to each protomer
571 are coloured differently. Hydrogen bonds and π -interactions are coloured as in B.
572 Important waters are represented as red spheres and calcium as a green sphere. Calcium
573 coordination is depicted in purple. (D) CoaB dimerization interface. Each protomer is
574 coloured as in C. (D)

575

576 **Figure 3: Regulation of MtbCoaBC by CoA and CoA thioesters.**

577 (A) Inhibition of MtbCoaBC by CoA, acetyl-CoA, malonyl-CoA and succinyl-CoA. (B)
578 Lineweaver-Burk plots showing the effect of varying the concentration of each substrate
579 in the presence of different concentrations of acetyl-CoA.

580

581 **Figure 4: Inhibition of MtbCoaBC by compounds 1b and 2b.**

582 (A) Dose response profiles and chemical structure of compounds **1b** and **2b** is shown. (B)
583 Lineweaver-burke plots showing the effect of varying concentrations of compound **1b**
584 (left) and **2b** (right) in the presence of varying concentrations of CTP, PPA and L-
585 cysteine.

586

587 **Figure 5: MsmCoaB X-ray structure showing the cryptic allosteric site.**

588 CoaB with the cryptic allosteric site closed (A) and opened conformation (B) with
589 compound **1b** (pink) bound. (C) Detailed view of the allosteric site with compound **1b**
590 (yellow) bound. The individual protomers of the CoaB dimer are coloured in green or
591 pink.. Hydrogen bonds are depicted in red, π -interactions are in grey, and hydrophobic
592 interaction in green. Important waters are represented as red spheres and calcium as a
593 green sphere. Calcium coordination is depicted in purple. (D) Gating mechanism of the
594 cryptic allosteric site showing the movement of R207 with the closed conformation in
595 yellow and the open conformation in pink. An *E. coli* structure (PDB code: 1U7Z) with
596 the 4'-phosphopantothenoil-CMP (purple) intermediate bound is superimposed.

597

598 **Figure 6: Docking of compound 2b into MsmCoaB showing the highest scoring pose.**

599 Hydrogen bonds are shown in red. The individual protomers of the CoaB dimer are either
600 coloured in green or pink.

601

602

603

604

605 **Tables**

606

607 **Table 1:** Inhibition of CoaB domain by CoA, CoA thioesters and the most potent
608 inhibitors from of series one and two. IC₅₀ values determined using the EnzChek
609 pyrophosphate assay are shown.

Compound	IC₅₀ EnzCheck (μM)
CoA	148 \pm 11
AcCoA	121 \pm 9
MICoA	49 \pm 3
SucCoA	38 \pm 2
1b	0.28 \pm 0.05
1c	4.6 \pm 0.4
2b	0.08 \pm 0.01
2c	0.41 \pm 0.03
2d	0.54 \pm 0.06
2e	3.0 \pm 0.2

610

611 **Table 2:** Minimum inhibitory concentration (MIC) values of CoaB inhibitors against *M.*
612 *tuberculosis* H37Rv cultured in different media (μ M).

Compound	7H9/ADC/ Glycerol	7H9/ Cholesterol/ Tyloxapol	GAST/ Fe
1b	>250	>250	125
1c	>250	ND	ND
2b	>250	>250	50
2c	>250	>250	125
2d	>250	>250	ND
2e	>250	ND	ND

613 *ND – Not determined.

614

615

616

617

618

619 **Acknowledgements**

620 This work was funded by the Bill and Melinda Gates Foundation HIT-TB (OPP
621 OPP1024021) and SHORTEN-TB (OPP1158806) (VMendes and JCE) and in part by the
622 Intramural Research Program of NIH, NIAID (HIMB and CEB) and the South African
623 Medical Research Council and National Research Foundation (VMizrahi). CS was
624 funded in part by a NHMRC Overseas Biomedical Fellowship (1016357) with support
625 from the Bill and Melinda Gates Foundation HIT-TB (OPP OPP1024021). CoaBC
626 screening was funded by a MRC-CinC (grant no. MC_PC_14099). TLB is funded by the
627 Wellcome Trust (Wellcome Trust Investigator Award 200814_Z_16_Z: RG83114). The
628 authors would like to thank the Diamond Light Source for beam-time (proposals mx9537,
629 mx14043, mx18548) and the Seattle Structural Genomics Consortium for kindly
630 providing the *M. smegmatis* CoaB plasmid.

631

632 **References**

- 633 1. World Health, O. *Global tuberculosis report 2019*, (World Health Organization, Geneva,
634 2019).
- 635 2. Strauss, E. Coenzyme A Biosynthesis and Enzymology. *Comprehensive Natural Products*
636 *li: Chemistry and Biology, Vol 7: Cofactors*, 351-410 (2010).
- 637 3. Leonardi, R. & Jackowski, S. Biosynthesis of Pantothenic Acid and Coenzyme A. *EcoSal*
638 *Plus* **2**(2007).
- 639 4. Tsuchiya, Y. et al. Protein CoAlation and antioxidant function of coenzyme A in
640 prokaryotic cells. *Biochem J* **475**, 1909-1937 (2018).
- 641 5. Choudhary, C. et al. Lysine acetylation targets protein complexes and co-regulates
642 major cellular functions. *Science* **325**, 834-40 (2009).
- 643 6. Beld, J., Sonnenschein, E.C., Vickery, C.R., Noel, J.P. & Burkart, M.D. The
644 phosphopantetheinyl transferases: catalysis of a post-translational modification crucial
645 for life. *Nat Prod Rep* **31**, 61-108 (2014).
- 646 7. Wang, M. & Casey, P.J. Protein prenylation: unique fats make their mark on biology.
647 *Nat Rev Mol Cell Biol* **17**, 110-22 (2016).
- 648 8. Bird, J.G. et al. The mechanism of RNA 5' capping with NAD⁺, NADH and desphospho-
649 CoA. *Nature* **535**, 444-7 (2016).

- 650 9. Marrakchi, H., Laneelle, M.A. & Daffe, M. Mycolic acids: structures, biosynthesis, and
651 beyond. *Chem Biol* **21**, 67-85 (2014).
- 652 10. Guerrini, V. et al. Storage lipid studies in tuberculosis reveal that foam cell biogenesis
653 is disease-specific. *PLoS Pathog* **14**, e1007223 (2018).
- 654 11. Peyron, P. et al. Foamy macrophages from tuberculous patients' granulomas
655 constitute a nutrient-rich reservoir for *M. tuberculosis* persistence. *PLoS Pathog* **4**,
656 e1000204 (2008).
- 657 12. Evans, J.C. et al. Validation of CoaBC as a Bactericidal Target in the Coenzyme A
658 Pathway of *Mycobacterium tuberculosis*. *ACS Infect Dis* **2**, 958-968 (2016).
- 659 13. Kupke, T. et al. Molecular characterization of lantibiotic-synthesizing enzyme EpiD
660 reveals a function for bacterial Dfp proteins in coenzyme A biosynthesis. *J Biol Chem*
661 **275**, 31838-46 (2000).
- 662 14. White, M.D. et al. UbiX is a flavin prenyltransferase required for bacterial ubiquinone
663 biosynthesis. *Nature* **522**, 502-6 (2015).
- 664 15. Blaesse, M., Kupke, T., Huber, R. & Steinbacher, S. Crystal structure of the peptidyl-
665 cysteine decarboxylase EpiD complexed with a pentapeptide substrate. *EMBO J* **19**,
666 6299-310 (2000).
- 667 16. Blaesse, M., Kupke, T., Huber, R. & Steinbacher, S. Structure of MrsD, an FAD-binding
668 protein of the HFCD family. *Acta Crystallogr D Biol Crystallogr* **59**, 1414-21 (2003).
- 669 17. Albert, A. et al. The X-ray structure of the FMN-binding protein AtHal3 provides the
670 structural basis for the activity of a regulatory subunit involved in signal transduction.
671 *Structure* **8**, 961-9 (2000).
- 672 18. Manoj, N. & Ealick, S.E. Unusual space-group pseudosymmetry in crystals of human
673 phosphopantothenoylcysteine decarboxylase. *Acta Crystallogr D Biol Crystallogr* **59**,
674 1762-6 (2003).
- 675 19. Steinbacher, S. et al. Crystal structure of the plant PPC decarboxylase AtHAL3a
676 complexed with an ene-thiol reaction intermediate. *J Mol Biol* **327**, 193-202 (2003).
- 677 20. Stanitzek, S., Augustin, M.A., Huber, R., Kupke, T. & Steinbacher, S. Structural basis of
678 CTP-dependent peptide bond formation in coenzyme A biosynthesis catalyzed by
679 *Escherichia coli* PPC synthetase. *Structure* **12**, 1977-88 (2004).
- 680 21. Manoj, N., Strauss, E., Begley, T.P. & Ealick, S.E. Structure of human
681 phosphopantothenoylcysteine synthetase at 2.3 Å resolution. *Structure* **11**, 927-36
682 (2003).
- 683 22. Zheng, P. et al. Crystallographic Analysis of the Catalytic Mechanism of
684 Phosphopantothenoylcysteine Synthetase from *Saccharomyces cerevisiae*. *J Mol Biol*
685 (2019).
- 686 23. Kupke, T. Molecular characterization of the 4'-phosphopantothenoylcysteine
687 synthetase domain of bacterial dfp flavoproteins. *J Biol Chem* **277**, 36137-45 (2002).
- 688 24. Chan, D.S.-H. et al. Structural insights into *Escherichia coli*
689 phosphopantothenoylcysteine synthetase by native ion mobility–mass spectrometry.
690 *Biochemical Journal* **476**, 3125-3139 (2019).
- 691 25. Strauss, E., Kinsland, C., Ge, Y., McLafferty, F.W. & Begley, T.P.
692 Phosphopantothenoylcysteine synthetase from *Escherichia coli*. Identification and
693 characterization of the last unidentified coenzyme A biosynthetic enzyme in bacteria. *J*
694 *Biol Chem* **276**, 13513-6 (2001).
- 695 26. Awasthy, D. et al. Essentiality and functional analysis of type I and type III
696 pantothenate kinases of *Mycobacterium tuberculosis*. *Microbiology* **156**, 2691-701
697 (2010).
- 698 27. Song, W.J. & Jackowski, S. Kinetics and regulation of pantothenate kinase from
699 *Escherichia coli*. *J Biol Chem* **269**, 27051-8 (1994).
- 700 28. Vallari, D.S., Jackowski, S. & Rock, C.O. Regulation of pantothenate kinase by coenzyme
701 A and its thioesters. *J Biol Chem* **262**, 2468-71 (1987).

- 702 29. Wubben, T.J. & Mesecar, A.D. Kinetic, thermodynamic, and structural insight into the
703 mechanism of phosphopantetheine adenylyltransferase from *Mycobacterium*
704 *tuberculosis*. *J Mol Biol* **404**, 202-19 (2010).
- 705 30. Miller, J.R. et al. Phosphopantetheine adenylyltransferase from *Escherichia coli*:
706 investigation of the kinetic mechanism and role in regulation of coenzyme A
707 biosynthesis. *J Bacteriol* **189**, 8196-205 (2007).
- 708 31. Bennett, B.D. et al. Absolute metabolite concentrations and implied enzyme active site
709 occupancy in *Escherichia coli*. *Nat Chem Biol* **5**, 593-9 (2009).
- 710 32. Moolman, W.J., de Villiers, M. & Strauss, E. Recent advances in targeting coenzyme A
711 biosynthesis and utilization for antimicrobial drug development. *Biochem Soc Trans* **42**,
712 1080-6 (2014).
- 713 33. Kupke, T. Active-site residues and amino acid specificity of the bacterial 4'-
714 phosphopantothenoylcysteine synthetase CoaB. *Eur J Biochem* **271**, 163-72 (2004).
- 715 34. Yun, M. et al. Structural basis for the feedback regulation of *Escherichia coli*
716 pantothenate kinase by coenzyme A. *J Biol Chem* **275**, 28093-9 (2000).
- 717 35. Hartl, J., Kiefer, P., Meyer, F. & Vorholt, J.A. Longevity of major coenzymes allows
718 minimal de novo synthesis in microorganisms. *Nat Microbiol* **2**, 17073 (2017).
- 719 36. Nguyen, L. & Pieters, J. Mycobacterial subversion of chemotherapeutic reagents and
720 host defense tactics: challenges in tuberculosis drug development. *Annu Rev*
721 *Pharmacol Toxicol* **49**, 427-53 (2009).
- 722 37. Vonrhein, C. et al. Data processing and analysis with the autoPROC toolbox. *Acta*
723 *Crystallogr D Biol Crystallogr* **67**, 293-302 (2011).
- 724 38. Kabsch, W. Xds. *Acta Crystallogr D Biol Crystallogr* **66**, 125-32 (2010).
- 725 39. Evans, P.R. & Murshudov, G.N. How good are my data and what is the resolution? *Acta*
726 *Crystallographica Section D-Biological Crystallography* **69**, 1204-1214 (2013).
- 727 40. French, S. & Wilson, K. Treatment of Negative Intensity Observations. *Acta*
728 *Crystallographica Section A* **34**, 517-525 (1978).
- 729 41. Winn, M.D. et al. Overview of the CCP4 suite and current developments. *Acta*
730 *Crystallogr D Biol Crystallogr* **67**, 235-42 (2011).
- 731 42. McCoy, A.J. et al. Phaser crystallographic software. *J Appl Crystallogr* **40**, 658-674
732 (2007).
- 733 43. Adams, P.D. et al. PHENIX: a comprehensive Python-based system for macromolecular
734 structure solution. *Acta Crystallogr D Biol Crystallogr* **66**, 213-21 (2010).
- 735 44. Emsley, P., Lohkamp, B., Scott, W.G. & Cowtan, K. Features and development of Coot.
736 *Acta Crystallogr D Biol Crystallogr* **66**, 486-501 (2010).
- 737 45. Jubb, H.C. et al. Arpeggio: A Web Server for Calculating and Visualising Interatomic
738 Interactions in Protein Structures. *J Mol Biol* **429**, 365-371 (2017).
- 739 46. Singh, V. et al. The complex mechanism of antimycobacterial action of 5-fluorouracil.
740 *Chem Biol* **22**, 63-75 (2015).

741

742

743 **Author contributions**

744 VMendes wrote the manuscript. VM designed and performed all the crystallographic
745 experiments with the help of MB, OB and JCW. VMendes and JH designed and
746 performed the kinetic experiments. JH synthesised 4'-phosphopantothenate. PHMT

747 performed docking experiments. DSC performed the native mass spectrometry
748 experiments. SG, TB, SON, SD, JP and CS developed and performed the high-throughput
749 screening. JCE, SLL and HIMB performed the microbiology experiments on *M.*
750 *tuberculosis* H37Rv. VMendes, JCE, SG, AGC, PCR, KR, CA, HIMB, CEB, VMizrahi,
751 PGW and TLB managed the project. All authors approved the manuscript.

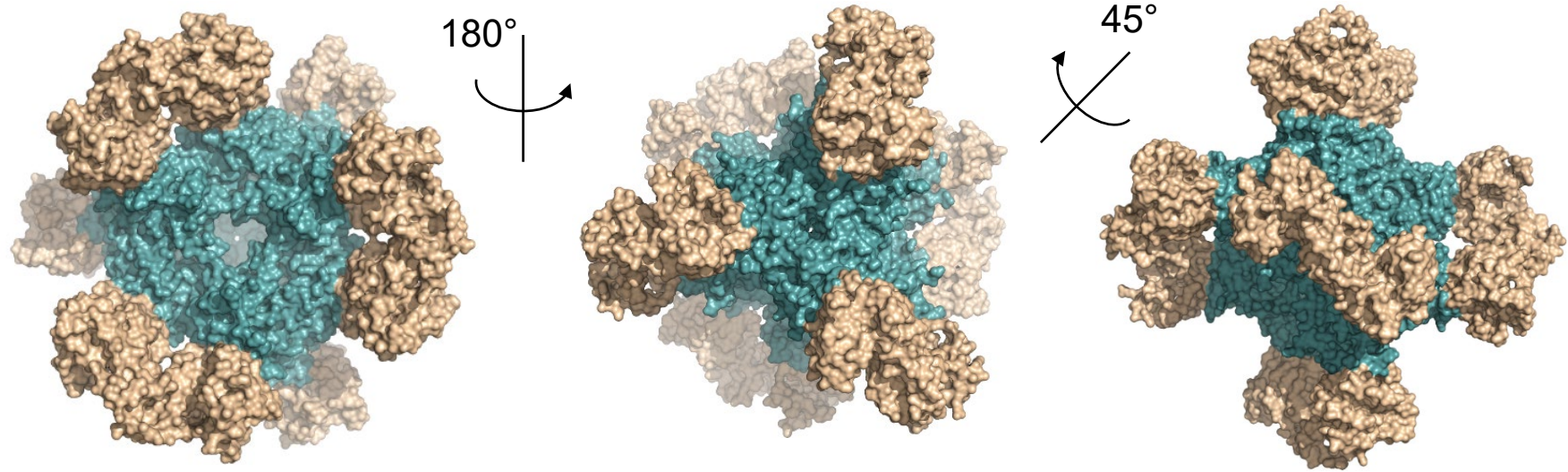
752

753 **Accession numbers**

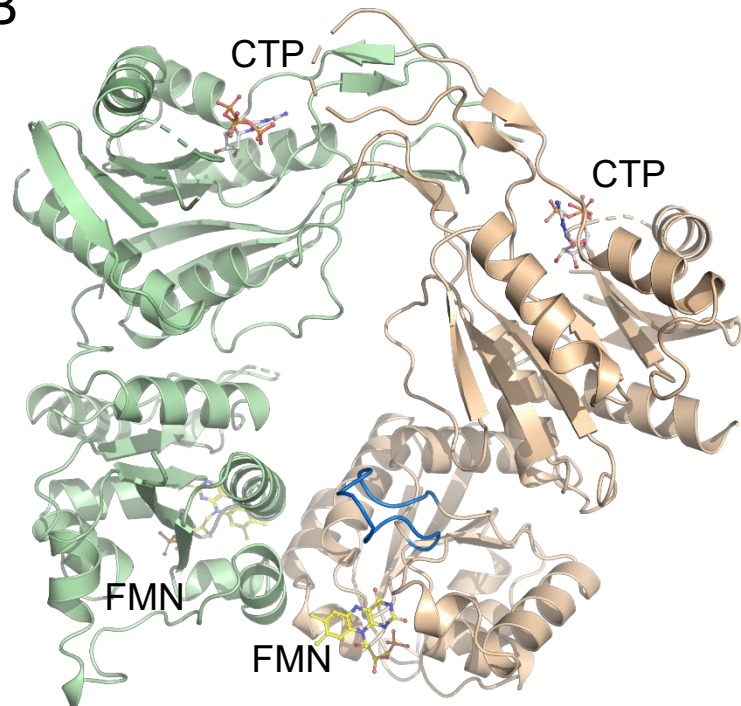
754 Coordinates and structure factors related to this work have been deposited in the PDB
755 with accession numbers: **6TGV**, **6TH2** and **6THC**.

Figure 1

A



B



C

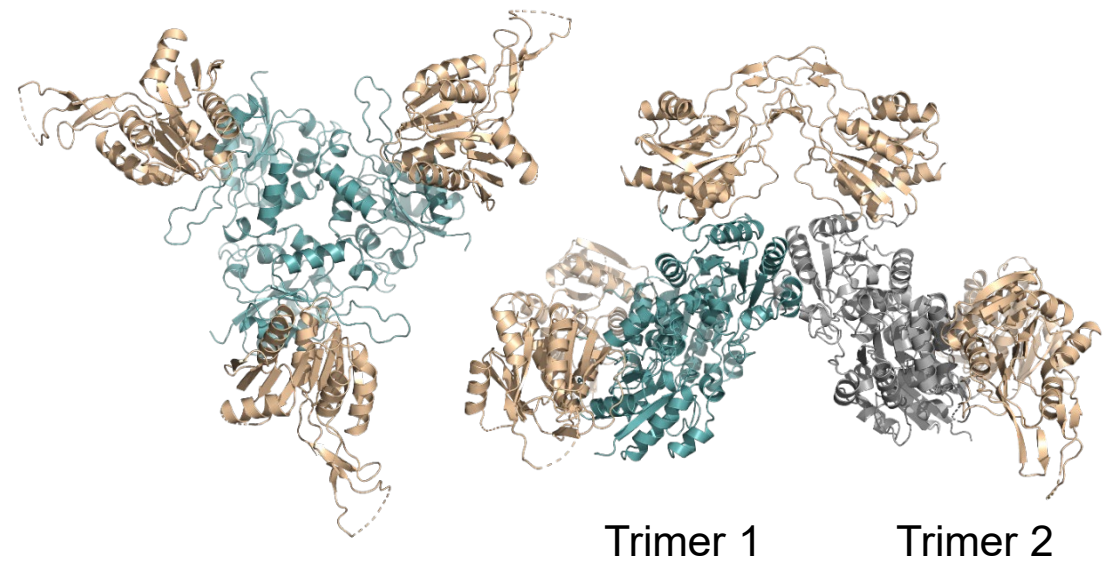


Figure 2

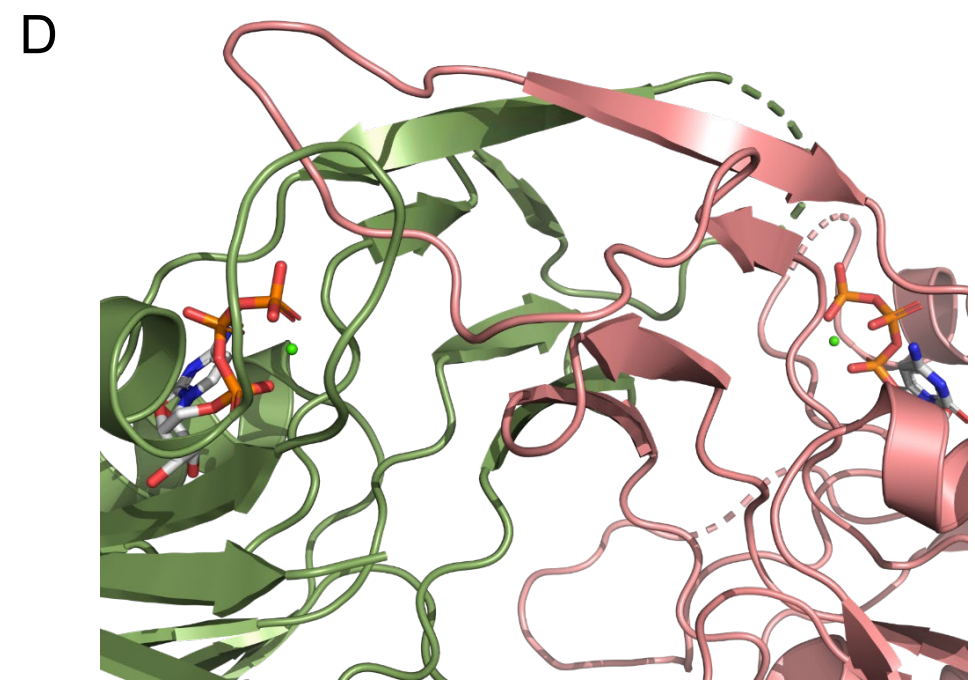
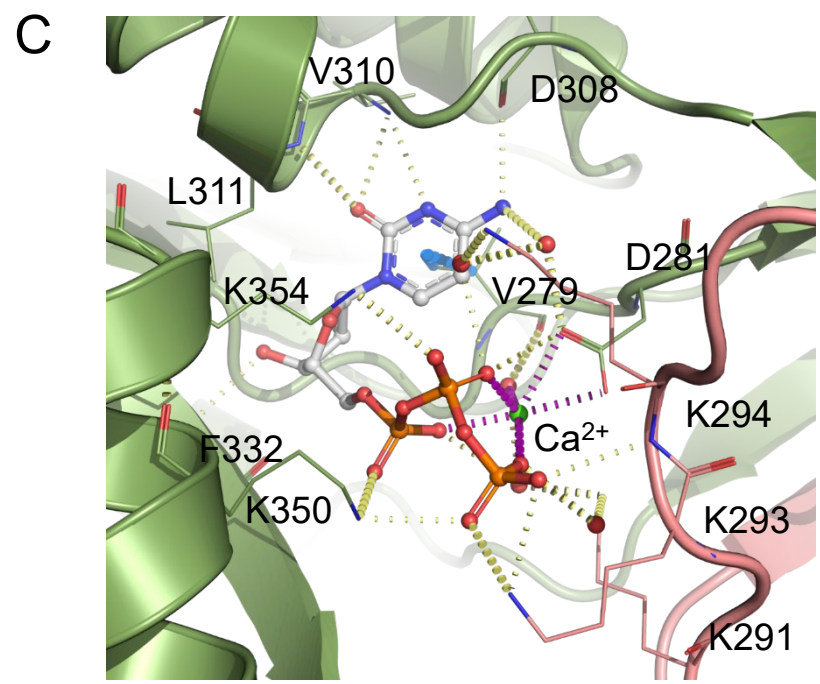
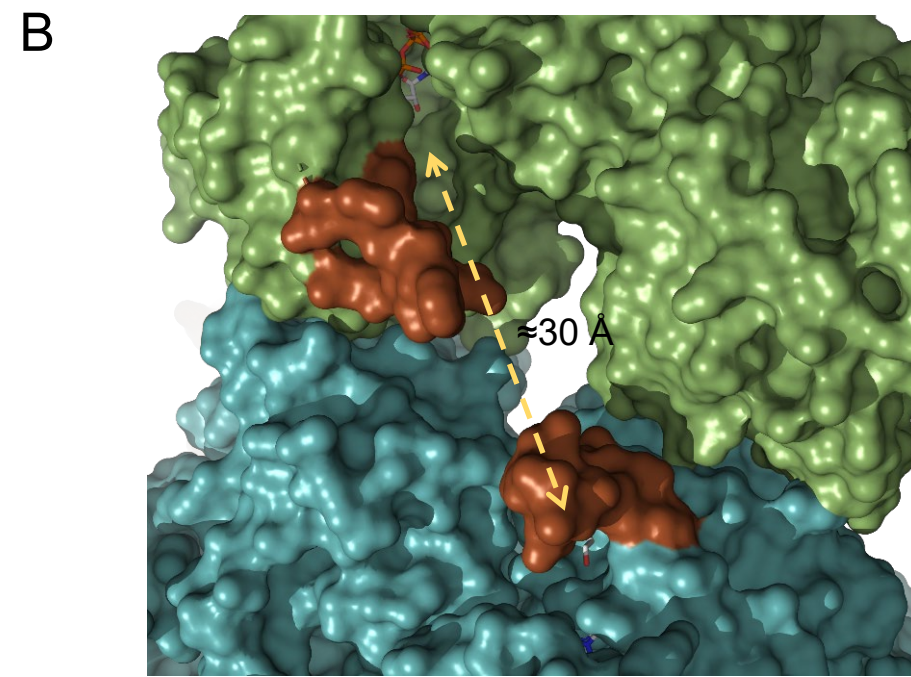
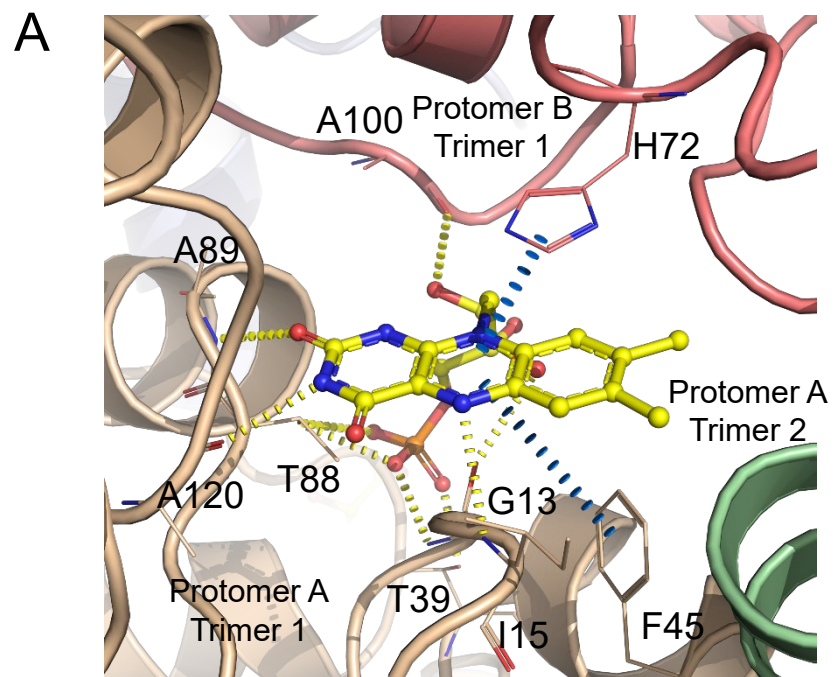
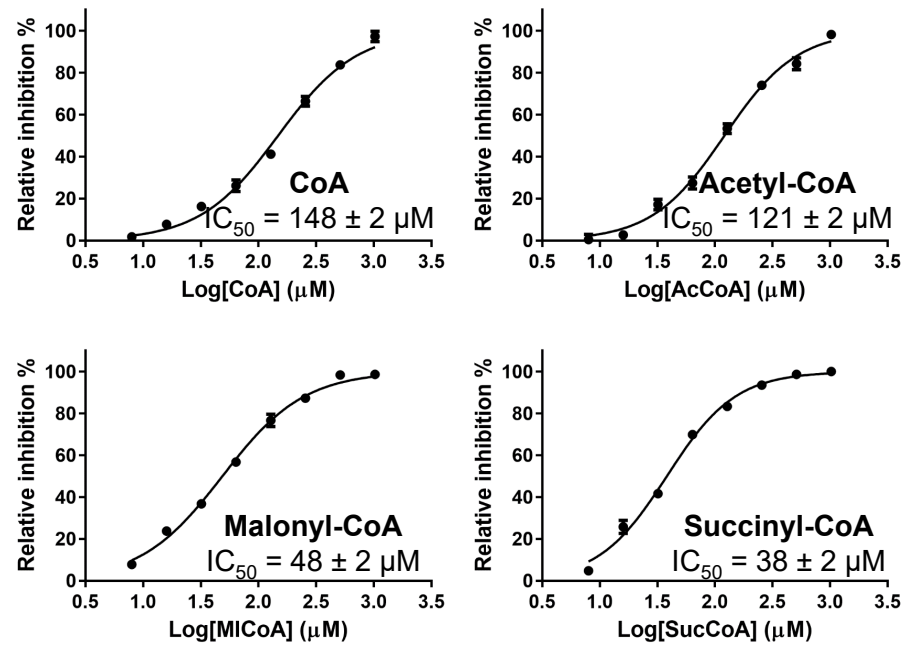


Figure 3

A



B

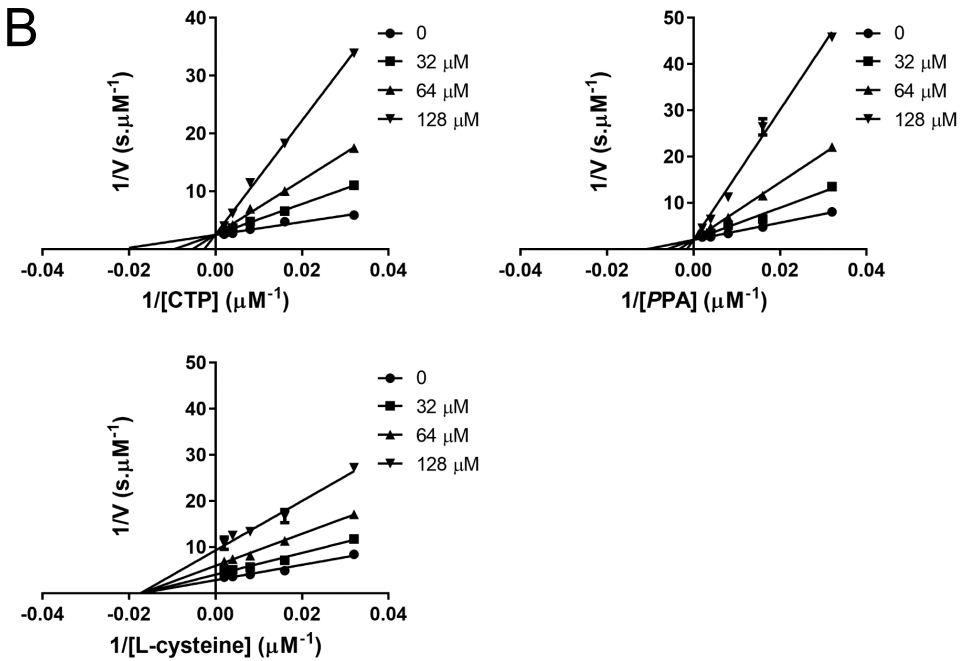
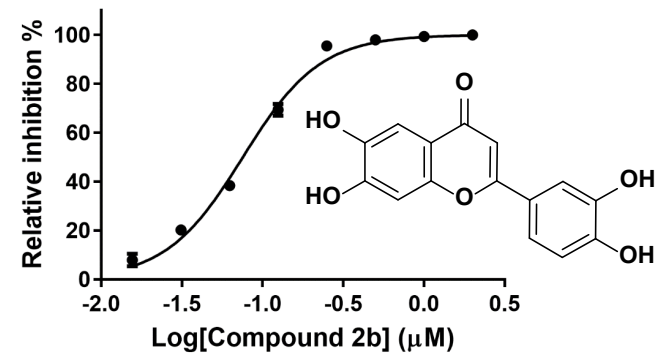
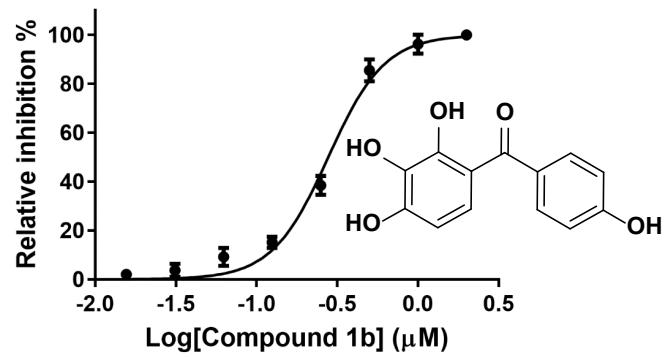


Figure 4

A



B

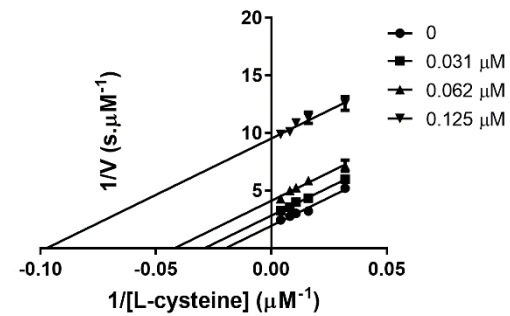
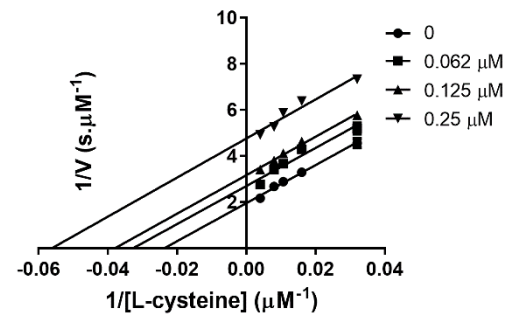
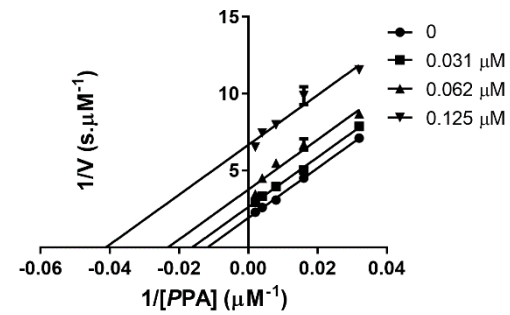
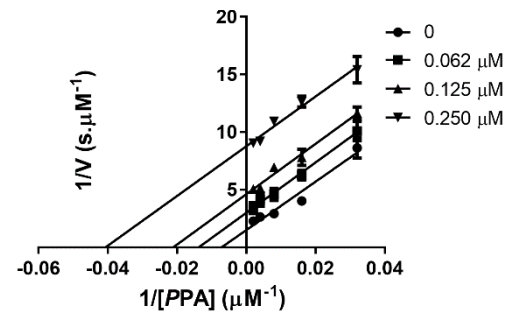
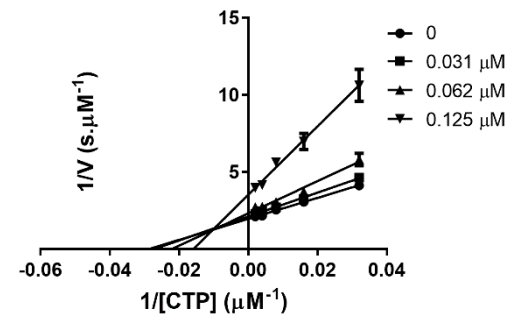
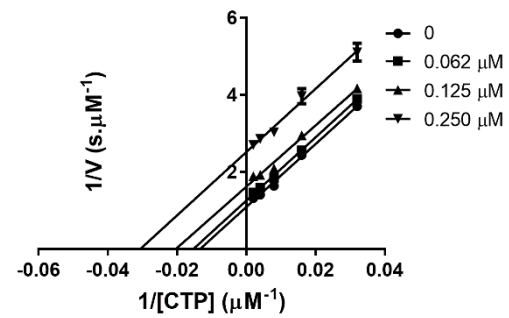


Figure 5

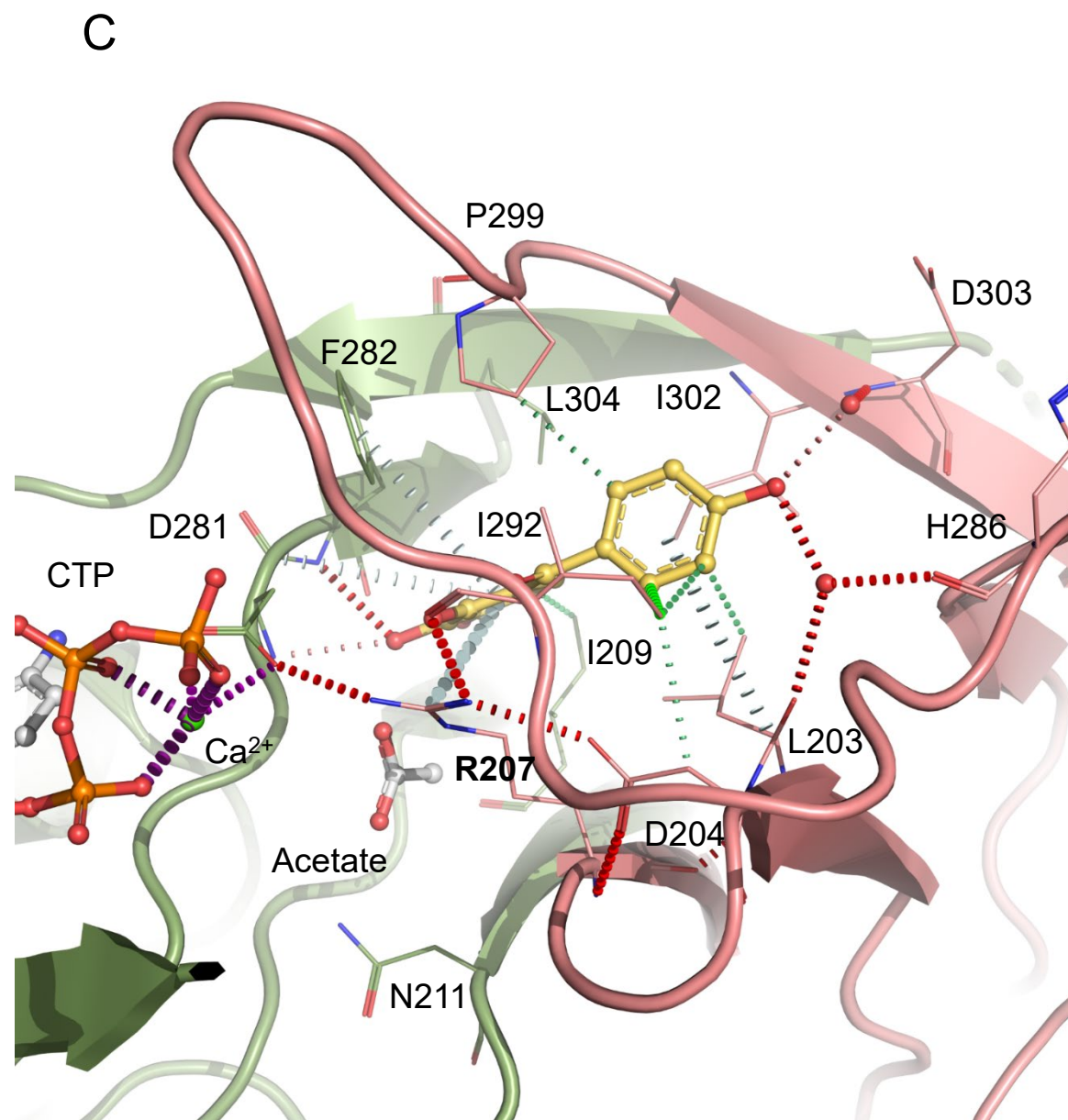
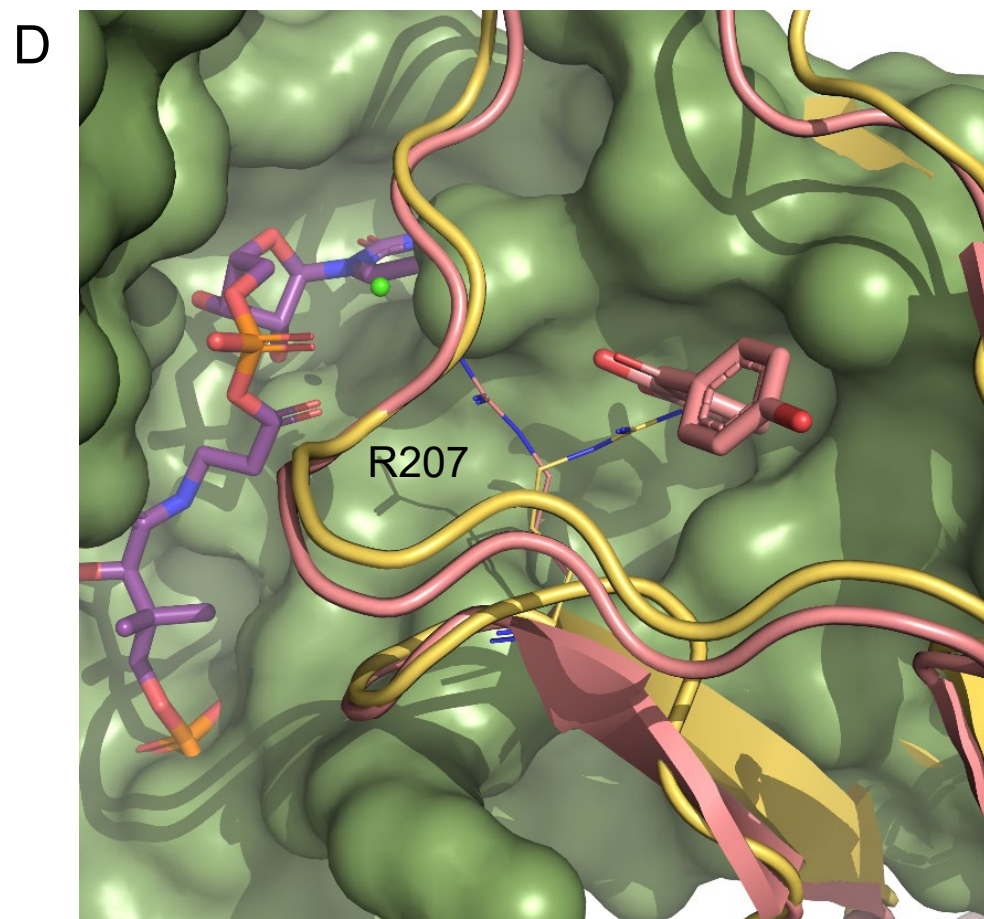
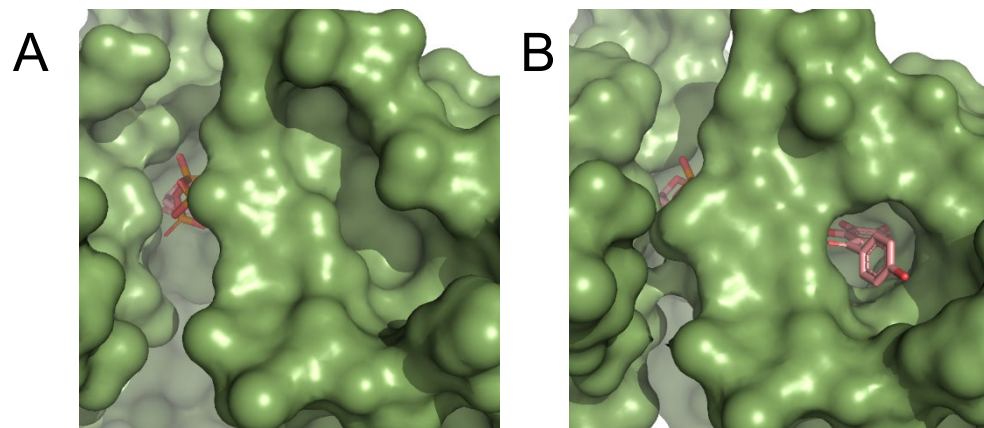


Figure 6

